

Emergence of ferroelectricity at the morphotropic phase boundary of ultrathin BiFeO₃

Johanna Nordlander,^{*} Aline Maillard, Manfred Fiebig, and Morgan Trassin[†]
Department of Materials, ETH Zurich, CH-8093 Zurich, Switzerland

We demonstrate the robustness of polarization in ultrathin compressive strained BiFeO₃ single layers and heterostructures during epitaxial thin-film growth. Using in-situ optical second harmonic generation (ISHG), we explore the emergence of ferroelectric phases at the strain-driven morphotropic phase boundary in the ultrathin regime. We find that the epitaxial films grow in the ferroelectric tetragonal (T-) phase without exhibition of a critical thickness. The robustness of this high-temperature T-phase against depolarizing-field effects is further demonstrated during the growth of capacitor-like (metal|ferroelectric|metal) heterostructures. Using temperature-dependent ISHG post-deposition, we identify the thickness-dependent onset of the monoclinic distortion in the T-matrix and trace the signature of the subsequent emergence of the strain-relaxed rhombohedral-like monoclinic phase. Our results show that strain-driven T-phase stabilization in BiFeO₃ yields a prominent candidate material for realizing ultrathin ferroelectric devices.

I. INTRODUCTION

Epitaxial strain engineering in complex-oxide thin films has proven an extremely successful path for designing materials with novel or enhanced functionality.¹ In the case of ferroelectric oxides, epitaxial strain leads to enhanced ordering temperatures, varying domain configurations and even new, metastable phases.^{2,3} A prototypical example for the immense impact epitaxial strain can have on ferroelectric properties is seen in BiFeO₃ (BFO) thin films. In this system, strain engineering led to the discovery of a strain-driven morphotropic phase boundary with a transition from the bulk-stable rhombohedral-like (R-like) monoclinic phase to a metastable tetragonal-like (T-like) monoclinic phase at compressive strain values exceeding 4%.⁴ The epitaxially stabilized T-like phase is in a so-called supertetragonal state with a c/a ratio ~ 1.2 and an unusually large spontaneous polarization of $150 \mu\text{C}/\text{cm}^2$ along the c -axis.⁵ Furthermore, because of the flat energy landscape around the morphotropic phase boundary in the phase diagram of BFO, such films tend to relax this strain state with increasing thickness through the formation and coexistence of several metastable monoclinic phases, bridging the transition from T-like to R-like. In this mixed-phase region of the thickness-strain diagram, the system exhibits exceptionally pronounced piezoelectric and ferroelectric response under the application of an electric field.^{5,6}

Despite these promising features displayed by highly strained BFO, it is not yet understood how these metastable polar phases behave in the technologically relevant ultrathin regime. Such insight is essential to expedite their device implementation.⁷ Since BFO is ferroelectric at the epitaxial growth temperature,⁸ it is of particular importance to understand the interplay between strain and depolarizing-field effects on the formation of the ferroelectric state right in the growth environment in both single layers and device-like heterostructures.

Here, we use Ce_{0.04}Ca_{0.96}MnO₃ (CCMO-) buffered, (001)-oriented LaAlO₃ (LAO) as substrate (lattice mismatch of about -4.5%) in order to grow epitaxially strained BFO close to the morphotropic phase boundary.⁴ We use in-situ optical second harmonic generation (ISHG) during growth to probe the emergence of polarization.⁸ At the deposition temperature,

we find that the compressive strain imposed by the substrate results in the epitaxial growth of BFO in a purely tetragonal single-domain state for a thickness of up to at least 80 unit cells. Phase transitions related to the onset of monoclinic distortions are only observed upon sample cooling, where signatures of monoclinic distortion of the T-phase and formation of R-phase are identified at ca. 460°C and 200°C , respectively. We demonstrate zero critical thickness for tetragonal BFO on CCMO-buffered LAO. The single-domain polarization state of tetragonal BFO is preserved during capping with a top electrode in an ultrathin CCMO|BFO|CCMO capacitor heterostructure. The robustness of polarization in the ultrathin regime demonstrated in this work emphasizes the feasibility of supertetragonal BFO as a competitive candidate for ultrathin ferroelectric-based devices.

II. RESULTS

The BFO films are grown by pulsed laser deposition (PLD) on LAO substrates with and without the conducting CCMO buffer layer. The CCMO layer is grown at a substrate temperature of 700°C with an energy fluence of $1.15 \text{ J}/\text{cm}^2$ whereas BFO is deposited at 670°C with $1.3 \text{ J}/\text{cm}^2$ fluence. Both layers are grown at 0.15 mbar oxygen partial pressure. The CCMO layers are kept at a 15-unit-cell thickness so as to maintain the in-plane lattice parameter of the LAO substrate, i.e., 3.79 \AA , whereas the BFO layer thickness is varied from 10 to 80 unit cells. Layer thickness is controlled using in-situ reflection high-energy electron diffraction (RHEED) and post-deposition x-ray reflectivity. Reciprocal space mapping (RSM) by x-ray diffraction is used to characterize the phase and orientation of the thin films.

To probe the emergence of polarization in highly strained BFO, we monitor the ISHG response of the films during deposition in a reflection measurement geometry, as described in Ref. 8. SHG is a symmetry-sensitive nonlinear optical process leading to the emission of frequency-doubled light. This process depends on the point-group symmetry of the material, and is in particular sensitive to the symmetry breaking resulting from the onset or change of spontaneous polarization in a material.⁹⁻¹¹ In the electric-dipole approximation, SHG is

expressed by

$$P_i(2\omega) = \epsilon_0 \chi_{ijk}^{(2)} E_j(\omega) E_k(\omega), \quad (1)$$

where the indices i, j, k each take on coordinates x, y and z , P is the generated nonlinear polarization, ϵ_0 stands for the vacuum permittivity, $E_{j,k}$ are the electric-field components of the incident light and $\chi_{ijk}^{(2)}$ represents the material-dependent tensor components of the second-order susceptibility. The SHG intensity scales with the film thickness t as $I_{SHG} \propto |\chi^{(2)} t|^2$, where, the set of non-zero $\chi^{(2)}$ components is determined by the crystallographic point-group symmetry. In a ferroelectric like BFO, the magnitude of these tensor components is proportional to the spontaneous polarization. We take advantage of this symmetry and polarization sensitivity of SHG to monitor the polar state of the films. SHG has already proven efficient in distinguishing the different polar phases in strained BFO films earlier on.^{12–14} By combining the SHG probe with the thin-film deposition process, the in-situ nature of our technique now allows us to directly access the spontaneous polarization in BFO as it evolves during growth and to also follow the temperature-dependent phase transitions BFO experiences during post-deposition sample cooling in the growth chamber.

We first investigate the emergence of polarization in real time during the thin-film growth. Figure 1(a,b) displays the onset of ISHG, and, hence, of a spontaneous polarization, when BFO is deposited on CCMO-buffered LAO. Polarimetry of the ISHG signal [Fig. 1(a)] yields a symmetry compatible with a tetragonal point group with a polar axis normal to the thin-film surface. This observation holds during the growth of all films of this type in the thickness range of up to 80 unit cells investigated by us. In other words, we do not observe a symmetry-changing phase transition during the growth. We therefore postulate that the films are grown in the supertetragonal phase without monoclinic distortions.

Close inspection of the ISHG response at the early growth stages reveals an onset of SHG from the deposition of the very first monolayer. By normalizing the ISHG intensity to the film thickness, we extract the evolution of spontaneous unit-cell polarization of the film, $P_s \propto \chi^{(2)}$,⁸ during growth [Fig. 1(b)]. Clearly, the tetragonal BFO grown on CCMO-buffered LAO takes on its polarization from the very first unit-cell layer, remaining constant with increasing thickness. This is noteworthy because the polarization discontinuities at the top and bottom interfaces of a very thin ferroelectric layer leads to a very strong depolarizing field due to incomplete screening of bound charges.^{15–17} Consequently, ferroelectrics often exhibit a critical thickness below which the spontaneous polarization is either completely suppressed^{15,18} or coerced into a nanoscale multidomain state,^{19–21} such that the net polarization is quenched. In particular, R-like BFO has a critical thickness of five unit cells when grown on a conducting buffer, because of the incomplete screening of this depolarizing field.⁸ Here, in contrast, we demonstrate a complete absence of critical thickness with an immediate onset of the full polarization in the epitaxially stabilized supertetragonal phase.

To further investigate the apparent robustness of polarization in tetragonal BFO films against depolarizing field effects,

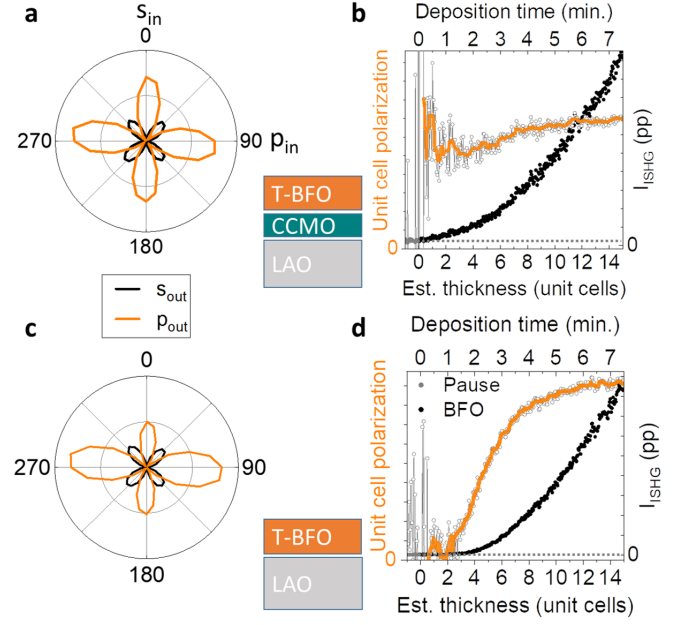


FIG. 1. ISHG measurements during BFO growth. (a,b) For BFO grown on CCMO-buffered LAO. (a) Polarimetry of the ISHG signal from BFO at the growth temperature. The polarization of the incident light is rotated from 0° to 360° , where 0° and 90° correspond to light polarized perpendicular to (s_{in}) and within (p_{in}) the plane of light reflection, respectively. The corresponding intensity of s-polarized (s_{out}) and p-polarized (p_{out}) SHG light is plotted in black and orange, respectively. The symmetry of the ISHG signal is compatible with a tetragonal ferroelectric state, and remains unchanged for film thicknesses up to at least 80 unit cells. (b) The ISHG signal for the p_{in} - p_{out} configuration during growth is shown in black. The dotted line represents the background SHG level. The extracted polarization of the film normalized by the film thickness in unit cells is shown in gray, where a floating average over 20 data points (orange) highlights the onset of the finite polarization directly at the start of the deposition, hence yielding a zero critical thickness. (c,d) For BFO grown directly on LAO. (c) ISHG polarimetry performed as in (a). Similarity to (a) confirms presence of the same type of tetragonal phase. (d) The ISHG response and corresponding polarization acquired as in (a) during growth reveals a 2-unit-cell critical thickness for the spontaneous polarization.

we next compare the emergence of polarization with and without electrical screening at the bottom interface. For this purpose, we keep the growth conditions as before, yet we omit the deposition of the CCMO bottom electrode, growing the BFO film directly on the insulating LAO substrate. In this case, we observe a delayed onset of the ISHG signal, corresponding to a threshold thickness for the emergence of polarization of two unit cells [Fig. 1(c)]. A critical thickness of less than 1 nm in the absence of depolarizing-field screening is a striking confirmation of the exceptional robustness of the polarization state in purely tetragonal BFO. Note that the ISHG polarimetry seen in Fig. 1(d) is identical to the case where BFO is grown on a CCMO buffer [Fig. 1(b)]. This confirms that the films are grown in the same supertetragonal phase in both cases.

The in-plane lattice parameter of 3.79 \AA imposed on the

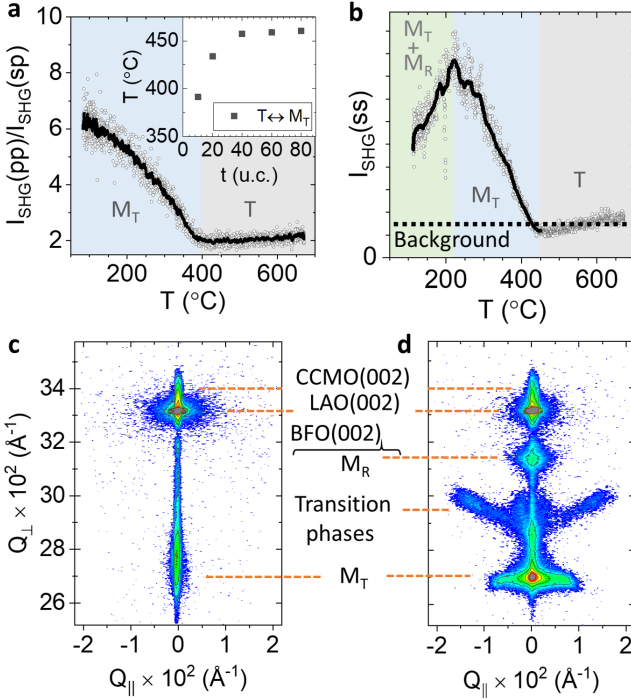


FIG. 2. (a,b) Temperature dependence of the ISHG signal during cooling of the BFO samples after deposition. (a) For a BFO film on CCMO-buffered LAO, a change of relative magnitude of $\chi^{(2)}$ components is observed at 390°C. We assign this change to the onset of monoclinic tilt of the polar axis in the T-phase and hence a phase transition to the M_T phase. As seen in the inset, thicker films on the same substrate exhibit this transition at higher temperatures, saturating around 460°C. (b) For films where our XRD characterization reveals the presence of R-phase, an additional symmetry change can be observed in the $s_{\text{in}}-s_{\text{out}}$ component around 200°C. This temperature is therefore attributed to the onset of formation of the monoclinic R-phase, here denoted M_R . (c,d) RSM around the (002) reflections of BFO films grown on CCMO-buffered LAO substrates with thicknesses of (c) 10 unit cells and (d) 80 unit cells confirms that the ultrathin films remain in the monoclinic T-phase down to room temperature, whereas strain-relaxation in thicker films promotes phase coexistence of monoclinic phases and inclusions of the R-like phase.

films by the substrates places the BFO close to the morphotropic phase boundary. Hence, whereas at the elevated growth temperature, the purely tetragonal phase of the BFO films prevails, we expect a development of phase coexistence towards room temperature.⁴ To follow the temperature-dependent evolution of the polarization in the thin films, we investigate the ISHG response for different film thicknesses during post-deposition cooling of the samples in the growth chamber. Since the onset of a monoclinic distortion corresponds to a reduction of the point-group symmetry from $4mm$ in the tetragonal phase to m in the monoclinic phases, such transitions are accompanied by new as well as modified components in the $\chi^{(2)}$ tensor. Therefore a corresponding change in the SHG contributions from the BFO film is expected.^{12–14}

By tracking different $\chi^{(2)}$ tensor components, we thus identify two transition temperatures (Fig. 2). The first transition is observed in the range of 460°C down to 390°C and the second

transition occurs around 200°C. With the excellent agreement of these transition temperatures with values reported in literature from scanning-probe and x-ray diffraction studies,^{22–24} we can assign the high-temperature transition to the point at which the strain-stabilized, purely tetragonal phase develops a monoclinic tilt (here labeled as M_T), see Fig. 2(a). The second transition then represents the formation of monoclinic R-like phase inclusions (here labeled as M_R), leading to a $M_R + M_T$ phase coexistence. The transition to the M_T phase is seen in all films and its transition temperature exhibits a dependence on film thickness, where thinner films exhibit a lower transition point [see inset in Fig. 2(a)]. In contrast, signatures of the low-temperature transition related to the emerge of M_R inclusions are only observed for films with higher thicknesses, where indeed we also see the presence of M_R inclusions at room-temperature by piezo-response force microscopy (not shown) and RSM [Fig. 2(c,d)]. Transition to this state during post-deposition cooling further indicates that R-phase inclusions are absent during the deposition itself so that the films remain coherently strained to the substrate throughout the growth process. It also serves as additional proof that the films are grown in the purely tetragonal phase in absence of monoclinic distortion up to thicknesses of at least 80 unit cells.

Next, we investigate the robustness of polarization in this supertetragonal phase after insertion into a capacitor-like heterostructure. The addition of a capping layer on top of an ultrathin ferroelectric film can often result in effects that are detrimental to an out-of-plane oriented polarization,¹⁵ such as drastically different electrostatic boundary conditions at the new interface. For instance, a transient enhancement of the depolarizing field might emerge during the epitaxial deposition of the top electrode.²¹ Such depolarizing-field effects can lead to abrupt domain splitting and a loss of net polarization in the capacitor, even if the ferroelectric layer was initially grown in a single-domain state. Here, we monitor the ISHG response during growth of a 20-unit-cell tetragonal BFO film and the subsequent deposition of a CCMO capping layer, which in total results in a CCMO|BFO|CCMO architecture. As seen in Fig. 3(a,b), the ISHG intensity related to the single-domain polarization in the tetragonal BFO films exhibits a slow, continuous reduction by about 50% during deposition of the CCMO top layer. This decrease cannot be solely attributed to optical losses due to the 5.5 nm thick CCMO layer. It is also incompatible, however, with an immediate quench of net polarization as it is expected for depolarizing-field-induced domain splitting.²¹ The unperturbed tetragonal symmetry throughout the growth of the CCMO electrode indicated by the ISHG polarimetry in Fig. 3(a,b) further excludes that nucleation of the R-like phase with its lower spontaneous polarization occurs. We finally note that the onset of monoclinic distortions is only observed when cooling down the sample [Fig. 3(c)]. Post-deposition RSM on films with and without CCMO capping reveals, however, that the electrode deposition results in a reduction of the BFO tetragonality of about 15 %, from 1.20 to 1.17 [Fig. 3(d,e)]. We attribute this decrease in the c lattice parameter to a residual influence of the depolarizing field,¹⁹ causing the polarization reduction in the tetragonal BFO and hence accounting for the reduction of that

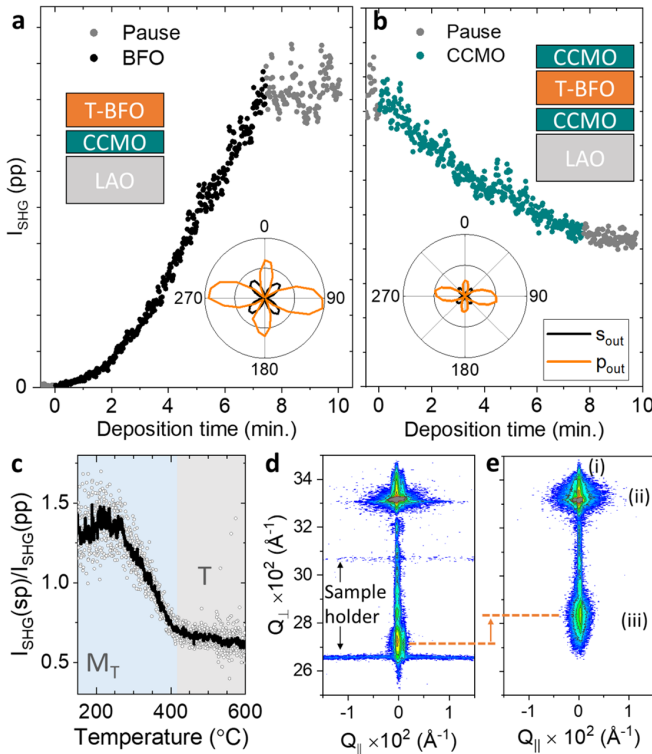


FIG. 3. (a,b) ISHG measurement of polarization in tetragonal BFO during deposition of a multilayer system. (a) Deposition of the first BFO layer on a CCMO buffer yields zero critical thickness and deposition in the tetragonal phase. The film thickness is 20 unit cells. (b) A 15-unit-cell thick CCMO capping layer leads to a gradual reduction in ISHG intensity. The insets show ISHG polarimetry plots subsequent to the respective layer deposition. The films retain their symmetry after CCMO deposition and only an overall reduction in ISHG magnitude is observed. (c) SHG tracking during cooling of the capped BFO sample indicate a shift of the M_T phase transition to slightly lower temperature than in the corresponding uncapped samples. (d,e) RSM of the out-of-plane (002) reflections for a 20-unit-cell BFO on CCMO-buffered LAO, (d) without and (e) with a CCMO top layer. The peaks are labeled as (i) CCMO, (ii) LAO and (iii) BFO. A reduction of the c lattice parameter of BFO of about 2.5% is observed in the film after capping.

part of the ISHG intensity that is not associated to optical loss.

Remarkably, despite the ultrathin thickness of the BFO film, where domain splitting or complete polarization suppression would be expected in the presence of an unscreened depolarizing field, we note that a net polarization remains in the heterostructure.

Preliminary density-functional calculations support the robustness of the high temperature tetragonal phase against polarization suppression and multidomain splitting. We find that the energy cost of polarization reorientation is exceptionally high.²⁵ The combination of strain and high-temperature stabilization of the supertetragonal phase thus results in a preferred single domain state of our films. Hence, a global reduction of tetragonality, rather than a multidomain breakdown is the more favourable path to reduce the net polarization and, thus, the accumulation of unscreened bound charges at the interfaces. Yet, the high compressive strain imposed by both top and bottom CCMO layers seem to prevent a suppression loss of polarization. This leads to an unusually pronounced polarization at elevated temperature.

III. CONCLUSION

In summary, we have demonstrated an exceptional robustness of polarization in epitaxially stabilized supertetragonal BFO ultrathin films grown on CCMO-buffered LAO. Only upon sample cooling, the monoclinic phase transitions characteristic for the strain-driven morphotropic phase boundary in BFO are observed. We find that the high-temperature tetragonal phase of BFO has zero critical thickness on the conducting buffer layer and grows in a single-domain ferroelectric state. This single-domain state is even preserved under unfavorable electrostatic boundary conditions, such as when the ultrathin tetragonal BFO is incorporated in a heterostructure environment. Strikingly, this system hence displays a polar state that is most robust at the growth temperature, letting it prevail during heterostructure growth, whereas the monoclinic distortions and phase coexistence that facilitate low-energy switching of the ferroelectric state at room temperature conveniently occur post-growth, during cooling of the finalized specimen. Our findings thus prove the great potential of highly compressive strained BFO films for implementation in nanoelectronic devices such as ferroelectric tunnel junctions⁷ and ferroelectric field-effect transistors.

* johanna.nordlander@mat.ethz.ch

† morgan.trassin@mat.ethz.ch

¹ R. Ramesh and N. A. Spaldin, *Nature Materials* **6**, 21 (2007).

² D. G. Schlom, L.-Q. Chen, C.-B. Eom, K. M. Rabe, S. K. Streiffer, and J.-M. Triscone, *Annual Review of Materials Research* **37**, 589 (2007).

³ A. R. Damodaran, J. C. Agar, S. Pandya, Z. Chen, L. Dedon, R. Xu, B. Apgar, S. Saremi, and L. W. Martin, *Journal of Physics: Condensed Matter* **28**, 263001 (2016).

⁴ R. Zeches, M. Rossell, J. Zhang, A. Hatt, Q. He, C.-H. Yang, A. Kumar, C. Wang, A. Melville, C. Adamo, *et al.*, *Science* **326**,

977 (2009).

⁵ J. Zhang, Q. He, M. Trassin, W. Luo, D. Yi, M. D. Rossell, P. Yu, L. You, C. H. Wang, C. Kuo, *et al.*, *Physical Review Letters* **107**, 147602 (2011).

⁶ P. Sharma, K.-R. Kang, Y.-Y. Liu, B.-K. Jang, J.-Y. Li, C.-H. Yang, and J. Seidel, *Nanotechnology* **29**, 205703 (2018).

⁷ H. Yamada, V. Garcia, S. Fusil, S. Boyn, M. Marinova, A. Gloter, S. Xavier, J. Grollier, E. Jacquet, C. Carrétéro, C. Deranlot, M. Bibes, and A. Barthélémy, *ACS Nano* **7**, 5385 (2013).

⁸ G. De Luca, N. Strkalj, S. Manz, C. Bouillet, M. Fiebig, and M. Trassin, *Nature Communications* **8**, 1419 (2017).

- ⁹ M. Fiebig, V. V. Pavlov, and R. V. Pisarev, *Journal of the Optical Society of America B* **22**, 96 (2005).
- ¹⁰ S. A. Denev, T. T. A. Lummen, E. Barnes, A. Kumar, and V. Gopalan, *Journal of the American Ceramic Society* **94**, 2699 (2011).
- ¹¹ J. Nordlander, G. De Luca, N. Strkalj, M. Fiebig, and M. Trassin, *Applied Sciences* **8**, 570 (2018).
- ¹² A. Kumar, S. Denev, R. J. Zeches, E. Vlahos, N. J. Podraza, A. Melville, D. G. Schlom, R. Ramesh, and V. Gopalan, *Applied Physics Letters* **97**, 112903 (2010).
- ¹³ R. C. Haislmaier, N. J. Podraza, S. Denev, A. Melville, D. G. Schlom, and V. Gopalan, *Applied Physics Letters* **103**, 031906 (2013).
- ¹⁴ M. Trassin, G. D. Luca, S. Manz, and M. Fiebig, *Advanced Materials* **27**, 4871 (2015).
- ¹⁵ J. Junquera and P. Ghosez, *Nature* **422**, 506 (2003).
- ¹⁶ A. K. Tagantsev and G. Gerra, *Journal of Applied Physics* **100**, 051607 (2006).
- ¹⁷ C.-L. Jia, V. Nagarajan, J.-Q. He, L. Houben, T. Zhao, R. Ramesh, K. Urban, and R. Waser, *Nature Materials* **6**, 64 (2007).
- ¹⁸ D. D. Fong, G. B. Stephenson, S. K. Streiffer, J. A. Eastman, O. Auciello, P. H. Fuoss, and C. Thompson, *Science* **304**, 1650 (2004).
- ¹⁹ C. Lichtensteiger, J.-M. Triscone, J. Junquera, and P. Ghosez, *Physical Review Letters* **94**, 047603 (2005).
- ²⁰ C. Lichtensteiger, M. Dawber, N. Stucki, J.-M. Triscone, J. Hoffman, J.-B. Yau, C. H. Ahn, L. Despont, and P. Aebi, *Applied Physics Letters* **90**, 052907 (2007).
- ²¹ N. Strkalj, G. De Luca, M. Campanini, S. Pal, J. Schaab, C. Gattinoni, N. A. Spaldin, M. D. Rossell, M. Fiebig, and M. Trassin, *Physical Review Letters* **123**, 147601 (2019).
- ²² H.-J. Liu, C.-W. Liang, W.-I. Liang, H.-J. Chen, J.-C. Yang, C.-Y. Peng, G.-F. Wang, F.-N. Chu, Y.-C. Chen, H.-Y. Lee, L. Chang, S.-J. Lin, and Y.-H. Chu, *Physical Review B* **85**, 014104 (2012).
- ²³ A. R. Damodaran, S. Lee, J. Karthik, S. MacLaren, and L. W. Martin, *Physical Review B* **85**, 024113 (2012).
- ²⁴ C. Beekman, W. Siemons, T. Z. Ward, M. Chi, J. Howe, M. D. Biegalski, N. Balke, P. Maksymovych, A. K. Farrar, J. B. Romero, P. Gao, X. Q. Pan, D. A. Tenne, and H. M. Christen, *Advanced Materials* **25**, 5561 (2013).
- ²⁵ B. F. Grosso, N. A. Spaldin, in preparation.